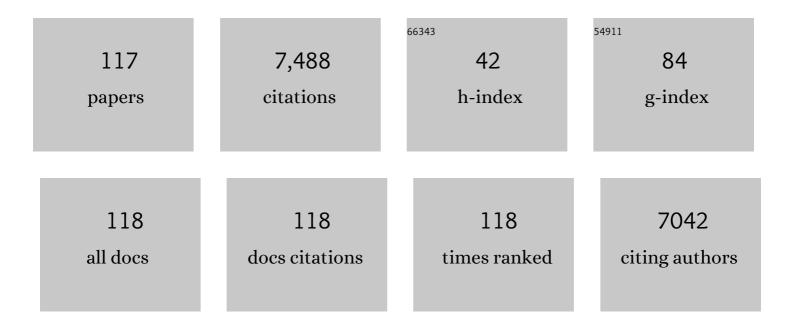
Yiping Guo

List of Publications by Year in descending order

Source: https://exaly.com/author-pdf/7301012/publications.pdf Version: 2024-02-01



YIDING GUO

#	Article	IF	CITATIONS
1	Excellent thermal stability and enhanced piezoelectric performance of Bi(Ni _{2/3} Nb _{1/3})O ₃ â€modified BiFeO ₃ –BaTiO ₃ ceramics. Journal of the American Ceramic Society, 2022, 105, 317-326.	3.8	14
2	Physical exercise promotes integration of grafted cells and functional recovery in an acute stroke rat model. Stem Cell Reports, 2022, 17, 276-288.	4.8	7
3	Hierarchically designed nanocomposites for triboelectric nanogenerator toward biomechanical energy harvester and smart home system. Nano Energy, 2022, 95, 107047.	16.0	23
4	Enhanced Visible Photocatalytic Hydrogen Evolution of KN-Based Semiconducting Ferroelectrics <i>via</i> Band-Gap Engineering and High-Field Poling. ACS Applied Materials & Interfaces, 2022, 14, 8916-8930.	8.0	18
5	Visible-light photocatalytic hydrogen production in a narrow-bandgap semiconducting La/Ni-modified KNbO ₃ ferroelectric and further enhancement <i>via</i> high-field poling. Journal of Materials Chemistry A, 2022, 10, 7238-7250.	10.3	18
6	Engineering the Defects and Microstructures in Ferroelectrics for Enhanced/Novel Properties: An Emerging Way to Cope with Energy Crisis and Environmental Pollution. Advanced Science, 2022, 9, e2105368.	11.2	46
7	Mechanically and electrically robust, electro-spun PVDF/PMMA blend films for durable triboelectric nanogenerators. Composites Part A: Applied Science and Manufacturing, 2022, 157, 106914.	7.6	25
8	Achieving Ultrahigh Photocurrent Density of Mg/Mn-Modified KNbO ₃ Ferroelectric Semiconductors by Bandgap Engineering and Polarization Maintenance. Chemistry of Materials, 2022, 34, 4274-4285.	6.7	15
9	Self-powered flexible piezoelectric sensors based on self-assembled 10Ânm BaTiOâ, f nanocubes on glass fiber fabric. Nano Energy, 2022, 99, 107400.	16.0	35
10	Bandgap-engineered ferroelectric single-crystalline NBT-BT based nanocomposites with excellent visible light-ultrasound catalytic performance. Chemosphere, 2022, 306, 135543.	8.2	7
11	Lead-free BiFeO3 film on glass fiber fabric: Wearable hybrid piezoelectric-triboelectric nanogenerator. Ceramics International, 2021, 47, 3573-3579.	4.8	37
12	Efficient induction of neural progenitor cells from human ESC/iPSCs on Type I Collagen. Science China Life Sciences, 2021, 64, 2100-2113.	4.9	3
13	Superflexible and Lead-Free Piezoelectric Nanogenerator as a Highly Sensitive Self-Powered Sensor for Human Motion Monitoring. Nano-Micro Letters, 2021, 13, 117.	27.0	57
14	Single-Nucleus Chromatin Accessibility Landscape Reveals Diversity in Regulatory Regions Across Distinct Adult Rat Cortex. Frontiers in Molecular Neuroscience, 2021, 14, 651355.	2.9	8
15	Dielectric Modulated Glass Fiber Fabricâ€Based Single Electrode Triboelectric Nanogenerator for Efficient Biomechanical Energy Harvesting. Advanced Functional Materials, 2021, 31, 2102431.	14.9	43
16	Hypoproliferative human neural progenitor cell xenografts survived extendedly in the brain of immunocompetent rats. Stem Cell Research and Therapy, 2021, 12, 376.	5.5	3
17	Highly-efficient piezocatalytic performance of nanocrystalline BaTi0.89Sn0.11O3 catalyst with Tc near room temperature. Nano Energy, 2021, 85, 106028.	16.0	56
18	Visible/near-infrared light absorbed nano-ferroelectric for efficient photo-piezocatalytic water splitting and pollutants degradation. Journal of Hazardous Materials, 2021, 416, 125808.	12.4	27

#	Article	IF	CITATIONS
19	Visuoauditory Associative Memory Established with Cholecystokinin Under Anesthesia Is Retrieved in Behavioral Contexts. Journal of Neuroscience, 2020, 40, 2025-2037.	3.6	14
20	Boosting the Photocatalytic Ability of Bandgap Engineered (Na _{0.5} Bi _{0.5})TiO ₃ –BaTiO ₃ by N–Ni Codoping. Journal of Physical Chemistry C, 2020, 124, 11810-11818.	3.1	26
21	Tailoring the Piezoelectric and Photoluminescence Properties of Na0.5Bi0.5TiO3-K0.5Bi0.5TiO3-BaTiO3-Based Multifunctional Ceramics with Sm Doping. Journal of Electronic Materials, 2020, 49, 4923-4928.	2.2	4
22	Visible or Near-Infrared Light Self-Powered Photodetectors Based on Transparent Ferroelectric Ceramics. ACS Applied Materials & Interfaces, 2020, 12, 33950-33959.	8.0	54
23	Highly piezoelectric lead-free ceramic powder: An efficient and eco-friendly multifunctional photocatalyst. Ceramics International, 2020, 46, 25266-25272.	4.8	7
24	Facile synthesis of mesoporous kaolin catalyst carrier and its application in deep oxidative desulfurization. Microporous and Mesoporous Materials, 2020, 306, 110415.	4.4	13
25	Facile synthesis of hierarchical TS-1 zeolite without using mesopore templates and its application in deep oxidative desulfurization. Microporous and Mesoporous Materials, 2019, 275, 61-68.	4.4	58
26	Understanding the Role of Oxygen Vacancy in Visible–Nearâ€Infraredâ€Lightâ€Absorbing Ferroelectric Perovskite Oxides Created by Offâ€Stoichiometry. Advanced Electronic Materials, 2019, 5, 1900407.	5.1	20
27	Direct auditory cortical input to the lateral periaqueductal gray controls sound-driven defensive behavior. PLoS Biology, 2019, 17, e3000417.	5.6	26
28	Trap-State Passivation by Nonvolatile Small Molecules with Carboxylic Acid Groups for Efficient Planar Perovskite Solar Cells. Journal of Physical Chemistry C, 2019, 123, 14223-14228.	3.1	40
29	Boosting piezoelectric response of KNNâ€based ceramics with strong visibleâ€light absorption. Journal of the American Ceramic Society, 2019, 102, 6422-6426.	3.8	29
30	Cholecystokinin release triggered by NMDA receptors produces LTP and sound–sound associative memory. Proceedings of the National Academy of Sciences of the United States of America, 2019, 116, 6397-6406.	7.1	38
31	Piezoelectric thin film on glass fiber fabric with structural hierarchy: An approach to high-performance, superflexible, cost-effective, and large-scale nanogenerators. Nano Energy, 2019, 59, 745-753.	16.0	54
32	Retrograde monosynaptic tracing through an engineered human embryonic stem cell line reveals synaptic inputs from host neurons to grafted cells. Cell Regeneration, 2019, 8, 1-8.	2.6	9
33	Piezoelectric Nanogenerators Based on Self-Poled Two-Dimensional Li-Doped ZnO Microdisks. Journal of Electronic Materials, 2019, 48, 2886-2894.	2.2	9
34	Design for Highly Piezoelectric and Visible/Nearâ€Infrared Photoresponsive Perovskite Oxides. Advanced Materials, 2019, 31, e1805802.	21.0	101
35	Synthesis of hierarchically porous TS-1 zeolite with excellent deep desulfurization performance under mild conditions. Microporous and Mesoporous Materials, 2018, 264, 272-280.	4.4	32
36	3D composites of ZnSnO3 nanoplates/reduced graphene oxide aerogels as an advanced lithium-ion battery anode. Journal of Materials Science: Materials in Electronics, 2018, 29, 5299-5306.	2.2	12

#	Article	IF	CITATIONS
37	MOF-Derived Hollow Co ₃ S ₄ Quasi-polyhedron/MWCNT Nanocomposites as Electrodes for Advanced Lithium Ion Batteries and Supercapacitors. ACS Applied Energy Materials, 2018, 1, 402-410.	5.1	69
38	Antagonism between the transcription factors NANOG and OTX2 specifies rostral or caudal cell fate during neural patterning transition. Journal of Biological Chemistry, 2018, 293, 4445-4455.	3.4	16
39	Selfâ€Healing Shape Memory PUPCL Copolymer with High Cycle Life. Advanced Functional Materials, 2018, 28, 1704109.	14.9	87
40	CoSe/Co nanoparticles wrapped by in situ grown N-doped graphitic carbon nanosheets as anode material for advanced lithium ion batteries. Journal of Power Sources, 2018, 399, 223-230.	7.8	70
41	Highâ€Coulombicâ€Efficiency Carbon/Li Clusters Composite Anode without Precycling or Prelithiation. Small, 2018, 14, e1802226.	10.0	31
42	Facile preparation of hierarchical titanium silicalite-1 (TS-1) with efficient oxidation of cyclic alkenes using PVA modified MWCNTs as templates. Journal of Alloys and Compounds, 2017, 699, 386-391.	5.5	23
43	Synthesis of Orthorhombic Perovskite-Type ZnSnO ₃ Single-Crystal Nanoplates and Their Application in Energy Harvesting. ACS Applied Materials & Interfaces, 2017, 9, 8271-8279.	8.0	105
44	Facile preparation of high-quality perovskites for efficient solar cells via a fast conversion of wet PbI ₂ precursor films. RSC Advances, 2017, 7, 22492-22500.	3.6	20
45	Li 3 PO 4 -added garnet-type Li 6.5 La 3 Zr 1.5 Ta 0.5 O 12 for Li-dendrite suppression. Journal of Power Sources, 2017, 354, 68-73.	7.8	150
46	Reaction mechanisms of lithium garnet pellets in ambient air: The effect of humidity and CO ₂ . Journal of the American Ceramic Society, 2017, 100, 2832-2839.	3.8	167
47	Composition induced rhombohedral–tetragonal phase boundary and high piezoelectric activity in (K) Tj ETQq1 Solid State Communications, 2017, 259, 29-33.	l 0.78431 1.9	4 rgBT /Ove 16
48	Sequential EMT-MET induces neuronal conversion through Sox2. Cell Discovery, 2017, 3, 17017.	6.7	19
49	Ternary oxide BaSnO3 nanoparticles as an efficient electron-transporting layer for planar perovskite solar cells. Journal of Alloys and Compounds, 2017, 722, 196-206.	5.5	32
50	A three dimensional sulfur/reduced graphene oxide with embedded carbon nanotubes composite as a binder-free, free-standing cathode for lithium–sulfur batteries. RSC Advances, 2017, 7, 43483-43490.	3.6	5
51	Fabricating fast triggered electro-active shape memory graphite/silver nanowires/epoxy resin composite from polymer template. Scientific Reports, 2017, 7, 5535.	3.3	26
52	In situ preparation of carbon/Fe 3 C composite nanofibers with excellent electromagnetic wave absorption properties. Composites Part A: Applied Science and Manufacturing, 2017, 92, 33-41.	7.6	75
53	Synthesis of hierarchical TS-1 zeolite via a novel three-step crystallization method and its excellent catalytic performance in oxidative desulfurization. Fuel, 2017, 188, 232-238.	6.4	65
54	Phase structure, microstructure, and piezoelectric properties of potassium-sodium niobate-based lead-free ceramics modified by Ca. Journal of Alloys and Compounds, 2017, 693, 950-954.	5.5	10

#	Article	IF	CITATIONS
55	5-HT2 receptors mediate functional modulation of GABAa receptors and inhibitory synaptic transmissions in human iPS-derived neurons. Scientific Reports, 2016, 6, 20033.	3.3	17
56	Oxygen vacancies induced self-assembling synthesis of V 4+ -BiVO 4 /rGO core-shell nanorods with enhanced water splitting efficiency and superior sewage purification capability. Applied Catalysis A: General, 2016, 526, 105-112.	4.3	12
57	The effect of annealing on a 3D SnO2/graphene foam as an advanced lithium-ion battery anode. Scientific Reports, 2016, 6, 19195.	3.3	112
58	Activation of 5-HT 2A/2C receptors reduces the excitability of cultured cortical neurons. Neuroscience Letters, 2016, 632, 124-129.	2.1	4
59	3D composites of layered MoS ₂ and graphene nanoribbons for high performance lithium-ion battery anodes. Journal of Materials Chemistry A, 2016, 4, 13148-13154.	10.3	47
60	Three dimensional Graphene aerogels as binder-less, freestanding, elastic and high-performance electrodes for lithium-ion batteries. Scientific Reports, 2016, 6, 27365.	3.3	49
61	A facile method to fabricate polyurethane based graphene foams/epoxy/carbon nanotubes composite for electro-active shape memory application. Composites Part A: Applied Science and Manufacturing, 2016, 91, 292-300.	7.6	43
62	Enhanced Photovoltaic Performance of Perovskite Solar Cells Using Polymer P(VDF-TrFE) as a Processed Additive. Journal of Physical Chemistry C, 2016, 120, 12980-12988.	3.1	81
63	Size-controlled synthesis of BiFeO3 nanoparticles by a facile and stable sol–gel method. Journal of Materials Science: Materials in Electronics, 2016, 27, 10803-10809.	2.2	6
64	Continuously enhanced photoactivity of hierarchical β-Bi2O3/Bi2S3 heterostructure derived from novel BiO2CH3 octagonal nanoplates. Applied Catalysis A: General, 2016, 514, 146-153.	4.3	26
65	Activation of 5-HT2A/C receptor reduces glycine receptor-mediated currents in cultured auditory cortical neurons. Amino Acids, 2016, 48, 349-356.	2.7	9
66	Ionic Conductivity and Air Stability of Al-Doped Li ₇ La ₃ Zr ₂ O ₁₂ Sintered in Alumina and Pt Crucibles. ACS Applied Materials & Interfaces, 2016, 8, 5335-5342.	8.0	229
67	Facile preparation of highly cost-effective BaSO4@BiVO4 core-shell structured brilliant yellow pigment. Dyes and Pigments, 2016, 128, 49-53.	3.7	34
68	Phase transition and piezoelectric properties of dense (K0.48,Na0.52)0.95Li0.05Sb Nb()O3-0.03Ca0.5(Bi0.5,Na0.5)0.5ZrO3 lead free ceramics. Journal of Alloys and Compounds, 2016, 664, 503-509.	5.5	28
69	Multistep sintering to synthesize fast lithium garnets. Journal of Power Sources, 2016, 302, 291-297.	7.8	68
70	Reprogramming somatic cells to cells with neuronal characteristics by defined medium both in vitro and in vivo. Cell Regeneration, 2015, 4, 4:12.	2.6	16
71	Fabrication of ultralight three-dimensional graphene networks with strong electromagnetic wave absorption properties. Journal of Materials Chemistry A, 2015, 3, 3739-3747.	10.3	219
72	A green method to prepare TiO ₂ /MWCNT nanocomposites with high photocatalytic activity and insights into the effect of heat treatment on photocatalytic activity. RSC Advances, 2015, 5, 13430-13436.	3.6	20

#	Article	IF	CITATIONS
73	Solvent-assisted growth of organic–inorganic hybrid perovskites with enhanced photovoltaic performances. Solar Energy Materials and Solar Cells, 2015, 143, 360-368.	6.2	14
74	Electro-active shape memory composites enhanced by flexible carbon nanotube/graphene aerogels. Journal of Materials Chemistry A, 2015, 3, 11641-11649.	10.3	85
75	An economic method to build a puffing instrument for drug application in vitro. Journal of Neuroscience Methods, 2015, 256, 122-126.	2.5	1
76	Facile synthesis of V ⁴⁺ self-doped, [010] oriented BiVO ₄ nanorods with highly efficient visible light-induced photocatalytic activity. Physical Chemistry Chemical Physics, 2014, 16, 24519-24526.	2.8	134
77	Time course of the dependence of associative memory retrieval on the entorhinal cortex. Neurobiology of Learning and Memory, 2014, 116, 155-161.	1.9	3
78	Enhanced Photovoltaic Performance in Polycrystalline BiFeO ₃ Thin Film/ZnO Nanorod Heterojunctions. Journal of Physical Chemistry C, 2014, 118, 15200-15206.	3.1	35
79	Photoelectrochemical response and electronic structure analysis of mono-dispersed cuboid-shaped Bi ₂ Fe ₄ O ₉ crystals with near-infrared absorption. RSC Advances, 2014, 4, 28209-28218.	3.6	29
80	Photovoltaic effect of TiO2 thick films with an ultrathin BiFeO3 as buffer layer. Applied Physics A: Materials Science and Processing, 2014, 117, 1301-1306.	2.3	4
81	Photoelectric properties of BiVO4 thin films deposited on fluorine doped tin oxide substrates by a modified chemical solution deposition process. International Journal of Hydrogen Energy, 2014, 39, 5569-5574.	7.1	18
82	Enhanced Photovoltaic Effect in BiVO ₄ Semiconductor by Incorporation with an Ultrathin BiFeO ₃ Ferroelectric Layer. ACS Applied Materials & Interfaces, 2013, 5, 6925-6929.	8.0	60
83	Preparation and Dielectric Characteristics of Semitransparent CoFe2O4–P(VDF-TrFE) Nanocomposite Films. Journal of Electronic Materials, 2013, 42, 734-738.	2.2	1
84	Evidence for oxygen vacancy or ferroelectric polarization induced switchable diode and photovoltaic effects in BiFeO ₃ based thin films. Nanotechnology, 2013, 24, 275201.	2.6	110
85	Encoding and Retrieval of Artificial Visuoauditory Memory Traces in the Auditory Cortex Requires the Entorhinal Cortex. Journal of Neuroscience, 2013, 33, 9963-9974.	3.6	24
86	Photovoltaic properties of BiFeO3 thin film capacitors by using Al-doped zinc oxide as top electrode. Materials Letters, 2013, 91, 359-361.	2.6	53
87	Photovoltaic effect of a bilayer thin film with (Na _{0.5} Bi _{0.5}) _{1â^²<i>x</i>} Ba _{<i>x</i>} TiO ₃ /BiFeC Journal Physics D: Applied Physics, 2013, 46, 365304.) <s⊉b⊗>3<!--</td--><td>sub2hetero<mark>st</mark></td></s⊉b⊗>	su b2 hetero <mark>st</mark>
88	Structural Disorder in the Key Lead-Free Piezoelectric Materials, and. Advances in Condensed Matter Physics, 2013, 2013, 1-5.	1.1	0
89	Enhanced photovoltaic properties in polycrystalline BiFeO3 thin films with rhombohedral perovskite structure deposited on fluorine doped tin oxide substrates. Materials Letters, 2012, 88, 140-142.	2.6	55
90	Dielectric and optical properties of BiFeO3–(Na0.5Bi0.5)TiO3 thin films deposited on Si substrate using LaNiO3 as buffer layer for photovoltaic devices. Journal of Alloys and Compounds, 2012, 513, 154-158.	5.5	19

#	Article	IF	CITATIONS
91	Optical properties of BiFeO3–(Na0.5Bi0.5)TiO3 thin films deposited on glass substrates by chemical solution deposition. Materials Letters, 2012, 71, 60-62.	2.6	9
92	Response of intergrown microstructure to an electric field and its consequences in the lead-free piezoelectric bismuth sodium titanate. Journal of Solid State Chemistry, 2012, 187, 309-315.	2.9	24
93	xmins:mmi="http://www.w3.org/1998/Wath/Wath/WathNiL" display="inline"> <mmi:mrow><mmi:mo stretchy="false">(<mmi:msub><mmi:mi) (math<="" 0.784314="" 1="" 10="" 50="" 667="" etqq1="" overlock="" rgbt="" td="" tf="" tj=""><td>nvariant="1 3.2</td><td>normal">Na<!--<br-->135</td></mmi:mi)></mmi:msub></mmi:mo </mmi:mrow>	nvariant="1 3.2	normal">Na <br 135
94	Large Electric Field-Induced Strain and Antiferroelectric Behavior in (1- <i>x</i>)(Na _{0.5} Bi _{0.5})TiO ₃ - <i>x</i> BaTiO ₃ Ceramics. Chemistry of Materials, 2011, 23, 219-228.	6.7	178
95	Antiferroelectric Phase and Pyroelectric Response in (NayBiz)Ti1â^'xO3(1â^'x)-xBaTiO3 Ceramics. Journal of the American Ceramic Society, 2011, 94, 1350-1353.	3.8	49
96	A correlated electron diffraction, <i>in situ</i> neutron diffraction and dielectric properties investigation of poled (1- <i>x</i>)Bi0.5Na0.5TiO3- <i>x</i> BaTiO3 ceramics. Journal of Applied Physics, 2011, 110, .	2.5	21
97	Dielectric and tunable properties of highly (110)-oriented (Ba0.65Sr0.35)TiO3 thin films deposited on Pt/LaNiO3/SiO2/Si substrates. Journal of Sol-Gel Science and Technology, 2009, 49, 66-70.	2.4	14
98	Ferroelectric and pyroelectric properties of (Na0.5Bi0.5)TiO3–BaTiO3 based trilayered thin films. Thin Solid Films, 2009, 517, 2974-2978.	1.8	39
99	Structure and electrical properties of trilayered BaTiO3/(Na0.5Bi0.5)TiO3–BaTiO3/BaTiO3 thin films deposited on Si substrate. Solid State Communications, 2009, 149, 14-17.	1.9	27
100	The performance of Pt bottom electrode and PZT films deposited on Al2O3 /Si substrate by using LaNiO3 film as an adhesion layer. Solid State Communications, 2008, 145, 413-417.	1.9	8
101	Dielectric and ferroelectric properties of highly (100)-oriented (Na0.5Bi0.5)0.94Ba0.06TiO3 thin films grown on LaNiO3/γ-Al2O3/Si substrates by chemical solution deposition. Solid State Sciences, 2008, 10, 928-933.	3.2	66
102	CHEMICAL SOLUTION DEPOSITION AND ELECTRICAL PROPERTIES OF (100)-PREDOMINANT BaTiO3 THICKER FILMS. Integrated Ferroelectrics, 2007, 88, 51-57.	0.7	3
103	Ferroelectric and pyroelectric properties of highly (110)-oriented Pb(Zr0.40Ti0.60)O3 thin films grown on Ptâ^•LaNiO3â^•SiO2â^•Si substrates. Applied Physics Letters, 2007, 90, 232908.	3.3	23
104	Thickness Dependence of Electrical Properties of Highly (100)-Oriented BaTiO3Thin Films Prepared by One-Step Chemical Solution Deposition. Japanese Journal of Applied Physics, 2006, 45, 855-859.	1.5	17
105	Dielectric and piezoelectric properties of highly (100)-oriented BaTiO3 thin film grown on a Pt/TiOx/SiO2/Si substrate using LaNiO3 as a buffer layer. Journal of Crystal Growth, 2005, 284, 190-196.	1.5	84
106	(Na0.5K0.5)NbO3–LiTaO3 lead-free piezoelectric ceramics. Materials Letters, 2005, 59, 241-244.	2.6	582
107	Dielectric and piezoelectric properties of lead-free (Na0.5K0.5)NbO3–SrTiO3 ceramics. Solid State Communications, 2004, 129, 279-284.	1.9	349
108	Ferroelectric-relaxor behavior of (Na0.5K0.5)NbO3-based ceramics. Journal of Physics and Chemistry of Solids, 2004, 65, 1831-1835.	4.0	82

#	Article	IF	CITATIONS
109	Structure and Electrical Properties of Lead-Free (Na0.5K0.5)NbO3-BaTiO3Ceramics. Japanese Journal of Applied Physics, 2004, 43, 6662-6666.	1.5	231
110	Phase transitional behavior and piezoelectric properties of (Na0.5K0.5)NbO3–LiNbO3 ceramics. Applied Physics Letters, 2004, 85, 4121-4123.	3.3	1,394
111	Electric-field-induced strain and piezoelectric properties of a high Curie temperature Pb(In1/2Nb1/2)O3–PbTiO3 single crystal. Materials Research Bulletin, 2003, 38, 857-864.	5.2	30
112	Dependence of high electric-field-induced strain on the composition and orientation of Pb(Mg1/3Nb2/3)O3–PbTiO3 crystals. Solid State Communications, 2003, 126, 347-351.	1.9	56
113	The phase transition sequence and the location of the morphotropic phase boundary region in (1 Å) Tj ETQq1 1 0	.784314 r 1.8	g&T_Overloo
114	Effect of composition and poling field on the properties and ferroelectric phase-stability of Pb(Mg1/3Nb2/3)O3–PbTiO3 crystals. Journal of Applied Physics, 2002, 92, 6134-6138.	2.5	99
115	Domain Configuration and Ferroelectric Related Properties of the (110)cubCuts of Relaxor-Based Pb(Mg1/3Nb2/3)O3–PbTiO3Single Crystals. Japanese Journal of Applied Physics, 2002, 41, 1451-1454.	1.5	40
116	Peculiar properties of a high Curie temperature Pb(In1/2Nb1/2)O3–PbTiO3 single crystal grown by the modified Bridgman technique. Solid State Communications, 2002, 123, 417-420.	1.9	67
117	Growth and piezoelectric properties of Pb(Mg1/3Nb2/3)O3–PbTiO3 crystals by the modified Bridgman technique. Solid State Communications, 2001, 120, 321-324.	1.9	76